



## Research article

# Investigation of plasma parameters, distributions, and optical emission for the anti-microbial performance of non-woven fabric under direct current glow discharge

Ahmed Rida Galaly<sup>a,\*</sup>, Nagia Dawood<sup>b</sup><sup>a</sup> Department of Engineering Science, Applied College, Umm Al-Qura University, Makkah 24381, Saudi Arabia<sup>b</sup> Physics Department, Faculty of Science, Taibah University, Al Madina Al Monawara 42363, Saudi Arabia

## ARTICLE INFO

## Keywords:

DC glow discharge  
Low-pressure plasma  
Inactivation of *E. coli*  
Survival curves  
Non-woven fabric

## ABSTRACT

The distribution of electron temperature  $T_e$  and density  $N_e$  for direct current glow plasma discharge was investigated, using a single Langmuir probe, inserted inside the plasma cell. The radial temperature distribution has the same values, except with a small increment variation at the cathode edge, and an axial decrement for the temperature  $T_e$  distribution profiles from the cathode fall region, passing the abnormal glow region, up to the faraway axial region.

The radial distribution of the electron density  $N_e$  has its highest value at the cathode, with very intense plasma at the cathode fall region, and more  $N_e$  decrement in the abnormal glow region, passing the abnormal glow region up to the faraway axial region. In the axial  $N_e$  distribution, an increase in  $N_e$  from the cathode fall region reaches maximum values in the abnormal glow region and decreases in the faraway axial region.

The optimal plasma surface treatment of non-woven silk fabric (n-WSF) can be achieved by utilizing a high plasma density and low energy of electrons to inactivate viable cells attached to (n-WSF) at very short application times, leading to complete inactivation, where the bacterial inactivation rate increases in the abnormal glow region. Based on analyses of the experimental data of initial and final densities of viable cells using survival curves in the abnormal glow discharge region, a dramatic inhibitory effect of plasma discharge on the residual survival microbe ratio was observed.

## 1. Introduction

Plasma physics studies the fourth state of matter with the highest ratio in the universe. Plasma can be created on Earth through various methods such as electrical discharge, laser ablation, chemical reactions, thermal methods, and nuclear reactions [1,2]. Owing to its wide temperature range, plasma technology is currently being used in various fields for different applications, such as surface etching, biomedicine, surface coating, surface modification, waste destruction, gas treatments, chemical synthesis, disinfection, sterilization, fabric treatment, and machining [3–5]. Over the past two decades, numerous articles have been published on non-thermal plasma glow discharges using atmospheric pressure of plasma jet (APPJ), radiofrequency (RF), and Direct Current (DC) for various applications such as etching, coating, disinfection, sterilization, medical applications, and woven and non-woven fabric

\* Corresponding author.

E-mail addresses: [argalaly@uqu.edu.sa](mailto:argalaly@uqu.edu.sa) (A.R. Galaly), [ndawood@taibahu.edu.sa](mailto:ndawood@taibahu.edu.sa) (N. Dawood).

treatment [6–8]. Additionally, many studies have focused on thermal plasma using plasma gasification reactors for the treatment of different wastes, solid, plastic, scrap tires, medical, and grey water, and plasma gasification is considered a source for energy recovery by converting different wastes into syngas, pyrolysis oil, diesel oil, carbon, and slug [9–12].

Several studies have investigated the inactivation factors of spore-forming bacteria using low-pressure plasmas. These studies compared the characteristics of low-pressure plasma between different working gases for sterilization purposes [13]. Most of these studies have focused on the influence of the non-thermal characteristics of cold plasma on the acceleration of the sterilization process, depending on the discharge conditions. *Escherichia coli*, a gram-negative bacterium found in various habitats, can cause a range of illnesses ranging from diarrhea to respiratory and urinary tract infections. The use of plasma to combat various bacterial genera is a new technique made possible by the low gas temperature, low pressure, and atmospheric pressure in the air. Diagnostic methods have been utilized to examine the interaction between non-thermal plasma and microbes generated in DC glow discharge under vacuum and the effects of UV rays and reactive species caused by heat on surface disinfection. Additionally, the role of cold plasmas in biological and environmental research has been studied [14–16].

Fabrics, made of polymer materials, are one of the most significant industrial products owing to their crucial role in everyday life. They have various applications, including household clothing, medical surgical gowns, and agricultural fabrics. Recently, there has been growing global interest in the production of multifunctional fabrics. This interest has led to exceptional properties, such as antibacterial properties, and is non-toxic to human cells.

The use of plasma and fabric technology has gained considerable attention due to the need to address the growing environmental concerns. Consequently, extensive research is being conducted on the application of cold plasma as an environmentally friendly physical agent [17]. Cold plasma is gaining acceptance not only from an ecological standpoint but also from an economic perspective. The exposure of fabric materials to DC glow discharge causes both physical and chemical alterations in the surface and near-surface layers. The reactive species generated in the glow discharge have a profound impact on the mechanical properties of the fabric, and these advancements in modern technological processes are crucial in addressing the escalating environmental challenges [18].

Plasma technology has been extensively utilized in diverse industrial applications owing to its exceptional efficiency, minimal ecological footprint, and simplicity. This has led to its widespread adoption in various environmental processes, including the treatment of living organisms on fabrics using cold plasmas. Cold plasma, which ensures both electrical and biological safety, is employed to alter the properties of the material surfaces. In the fabric industry, plasma technology is being developed for numerous purposes such as improving dimensional stability, imparting flame repellency, enabling self-cleaning capabilities, providing anti-bacterial qualities, and enhancing resistance to UV degradation [6,19].

The focus of our current research is the diagnostic technique of a DC glow discharge plasma sputtering device, which operates at low pressures through particle bombardment. Additionally, it has extensive applications in various industries and material surfaces owing to its environmentally friendly nature. These applications include cleaning, purification, and sterilization. Moreover, the study of basic gas discharge processes and the development and improvement of detection techniques for small gas plasma values have been conducted [7,20].

In this work, we specifically investigated the characteristics of the electron temperatures and densities in different axial and radial distributions for an argon discharge. To achieve this, we used a mesh cathode (MC) configuration within the plasma cell. The aim was to determine the optimal position for the nonwoven fabric sample, ensuring a homogeneous and suitable disinfection process.

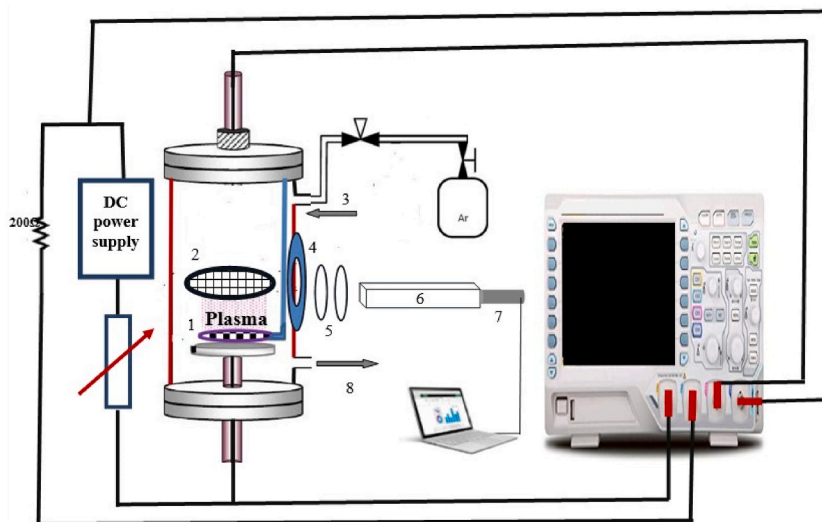


**Fig. 1.** The experimental set-up of the sputtering unit and the electrical circuit necessary to produce a glow discharge between two electrodes in a stainless tube with: 1) mesh cathode, 2) n-WSF with holder, 3) gas in, 4) glass windows, 5) lenses, 6) spectrometer, 7) CCD detector, and 8) vacuum.

## 2. Experimental set-up and procedures

### 2.1. Sputtering unit set-up

The experimental set-up of the sputtering unit and the electrical circuit necessary to produce a glow discharge between the two electrodes in a stainless tube with glass windows is illustrated in Fig. 1. In this set-up, argon gas was used as the working gas for various low-pressure glow discharges under breakdown. Furthermore, to generate a stationary DC glow discharge, several parameters were adjusted as follows: the discharge current ranged from 4 to 30 mA, the discharge DC voltage ranged from 200 to 1200 V, the pressure ranged from 1 to 5 mbar, and the current density ranged from 2 to 15 mA/m<sup>2</sup>. The emission from the MC plume to the bacterial colony samples attached to (n-WSF), was determined by capturing the light emitted from a DC plasma glow discharge system using an Avaspec-2048 spectrometer with a CCD (Charge Coupled Device) detector. The optical emission spectra of the emerging plasma plume above the MC were measured and showed lines and bands representing wavelengths ranging from 200 to 850 nm. Furthermore, the intensity emission spectra (IES) were also recorded.

The discharge chamber utilized in this study was the same as that previously employed by the author, as described in more detail in Refs. [21,22]. However, there is a difference in the diagnostic techniques employed, with the Faraday cup probe being replaced by a single probe [23]. The DC plasma source was operated using two parallel circular plate electrodes, with one electrode made of aluminum mesh serving as the cathode, and a copper electrode serving as the anode. These electrodes were positioned near each other with a small gap distance of 2 mm to prevent plasma formation between them. The plasma was confined above the mesh electrode, where the region of interest for the plasma study was located. To isolate the two electrodes from the stainless-steel outer chamber, a polytetrafluoroethylene (PTFE) insulating material was placed around them. This insulation confines the plasma over the mesh cathode (MC) and prevents the accumulation of charged sheaths on the electrode surfaces. The aluminum MC plays a crucial role in controlling the plasma, as will be discussed later. The number of holes per centimeter in the mesh configuration (which consists of a grid with seven wires per centimeter) allows for axial and radial measurements to control various parameters such as electron temperature, electron density, and ion velocity. These parameters are of great importance in sputtering processes, as they influence the rate, profile, reaction, and exposure time of the target sample, which floats in the plasma above the MC at different axial positions.

To measure the distribution of electron temperature  $T_e$  and density  $N_e$  in the direct current glow plasma discharge, a single-probe electric circuit was utilized in this study [24]. The circuit, as depicted in Fig. 2, consists of a single spherical probe made of phosphor bronze with a diameter of 2 mm. The probe diameter was kept as small as possible to minimize any potential disturbances to the plasma. In addition, the probe was cleaned by electron bombardment to reduce surface contamination. The probe was isolated using a thin glass tube, and the tip was immersed in glow discharge plasma. The probe was connected to a steady positive voltage ranging from 60 to 100 V to perform electron bombardment. The electrical circuit used for the single probe included a DC power supply, a 10-turn potentiometer (50 K), a load resistor ( $R_p = 1$  K), and a 10  $\mu$ F capacitor placed in parallel with the measuring resistor  $R_p$  to filter out noise. It is important to note that the axis of the single spherical Langmuir probe should always be positioned perpendicular to the electric field to avoid any distortion of the probe characteristics, especially in the vicinity of the space potential. The probe was periodically cleaned by ion bombardment to remove any possible hysteresis effects on the probe characteristics [25].

### 2.2. Culture media preparing

The culture media of the bacterial colonies adhered to the (n-WSF) samples were prepared before and after the antibacterial process using the DC plasma discharge system, and the Petri dishes were kept hidden at 10<sup>9</sup> CFU/mL (colonies formed per milliliter) *E. coli* from the contaminated sample without any sputtering [26,27].

To investigate the antibacterial properties of (n-WSF) samples, we experimented with the inactivation process of *Escherichia coli* (*E. coli* - gram-negative bacilli) attached to the samples. We tested various non-woven silk samples in the following ways. First, we prepared an overnight culture of approximately 10<sup>9</sup> cell-forming units per milliliter (cfu/ml) using untreated (n-WSF) samples as control Petri dishes that were not exposed to the plasma column above the MC.

Second, we tested the antimicrobial performance of the (n-WSF) samples after treatment for different exposure times with a viable

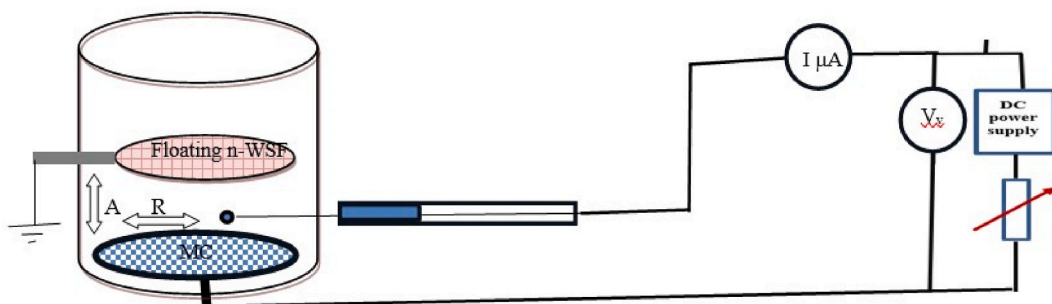


Fig. 2. Single probe electric circuit for measuring the axial (A) and radial (R) distribution of electron temperature  $T_e$  and density  $N_e$  in an evacuated chamber.

suspension of culture media. Finally, we spread *E. coli* onto a series of Petri dishes containing MacConkey agar medium (*Oxoid Australia, Adelaide, SA*) to assess the results [28]. From 15 (n-WSF) samples held perpendicular to the plasma column, each of the five samples was held at axial distances from the MC of 5 mm, 10 mm, and 15 mm at different exposure times, and one was kept as a control and not exposed [29].

The logarithm of the bacterial reduction (R) CFU/ml (the culture media of the bacterial colonies adhered to the (n-WSF) samples) was prepared before, and after the antibacterial process, taking into account the controller Petri dishes kept hidden with  $10^9$  CFU/mL (colonies formed per milliliter) *E. coli* [30], and the inactivation rate  $\eta\%$ , as a function of the plasma exposure time, where R,  $N_0$  and N are given by equation (1) [31]:

$$\text{Log (R)} = \text{Log}_{10} \left[ \frac{N_0}{N} \right] \quad (1)$$

The bacterial intensity before and after plasma treatment can be represented as  $N_0$  and N, respectively, in units of CFU/ml. The inactivation rate  $\eta$  can be calculated using Equation (2):

$$\text{Inactivation rate } \eta = \left[ \frac{N_0 - N}{N} \right] \times 100\% \quad (2)$$

### 2.3. Article structure arrangement

Table (1) shows an experimental roadmap for the antimicrobial control by DC glow discharge measurements, by studying the electrical characteristics, non-thermal characteristics, plasma modes, optical emission measurements, and anti-microbial measurements for the plasma plume incident on the (n-WSF).

## 3. Results and discussion

### 3.1. Potential and electric field distribution measurements

Potential distribution measurements were carried out by moving a single probe across the plasma cell with axial motion concerning one of the electrodes. These measurements were performed at a discharge current of 10 mA and a gas pressure ranging from 1 to 4 mbar for argon (Ar). The results in Fig. 3 illustrate that the potential distribution can be divided into three distinct regions.

In region I (AB), the potential rapidly increases over a short discharge length. This was attributed to the occurrence of gas breakdown within the tube, leading to a sudden increase in the ionization rate, particularly in the vicinity of the mesh cathode. Owing to their larger masses, positive ions move more slowly in an electric field than in electrons. Consequently, electrons are swiftly drawn toward the sample inside the plasma, leaving behind a dense positive space charge near the mesh cathode. Consequently, the electric field becomes distorted, and a significant portion of the applied potential is concentrated in the narrow space in front of the mesh cathode. In region II (BC), the potential exhibits a slight decrease, indicating a weaker electric field. This could be attributed to the presence of numerous free electrons in this region. In Region III (CD), the potential distribution remains nearly constant and linear. This is because the densities of positive and negative carriers are approximately equal in this region [32].

The measured potential distribution curves in Fig. 3 were differentiated to determine the values of the electric field (E). The formula used to calculate the electric field is as follows [33]:

$$E = (\Delta V_p / \Delta x) \quad (3)$$

Fig. 4 shows the distribution of the electric field at a discharge current of 10 mA and gas pressures ranging from 1 to 4 mbar. A high electric field was observed, which decreased sharply as one moved away from MC. This phenomenon can be attributed to the presence

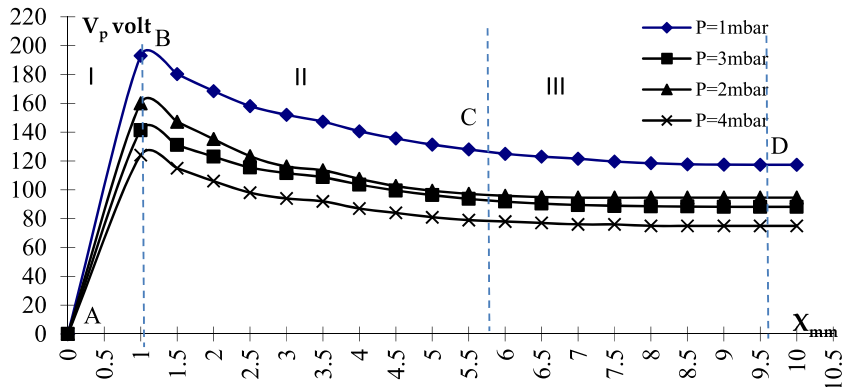


Fig. 3. The axial potential distribution measurements at a discharge current of 10 mA and an argon gas pressure ranging from 1 to 4 mbar.

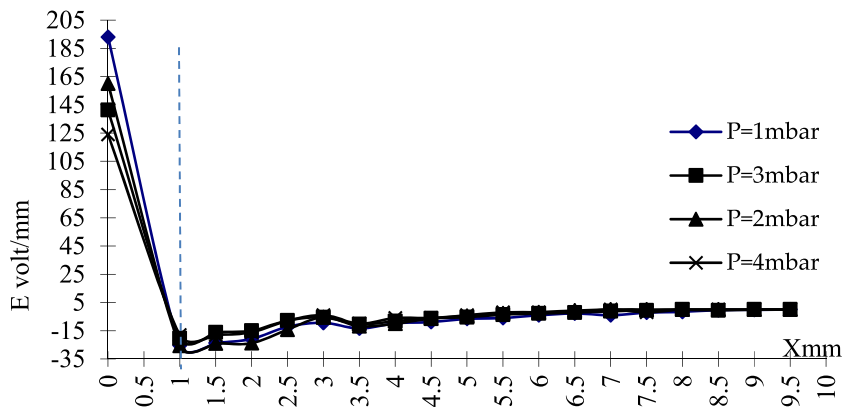


Fig. 4. The axial electric field distribution measurements at a discharge current of 10 mA and an argon gas pressure ranging from 1 to 4 mbar.

of an intense positive space charge in front of the MC. This space charge acts as an accelerator for the electrons toward the sample, and the kinetic energy gained by the electrons is dissipated through collisions with gas atoms near the sample, resulting in the production of secondary electrons [8].

### 3.2. Current-voltage characteristic of the single probe

The current-voltage characteristic curves of the single probe are depicted in Figures (5) and (6). These curves illustrate the behavior of the probe in two different axial regions: 4 mm near the MC and axially away further by 12 mm. The electrical characteristics of the discharge current were kept constant at 10 mA, while the argon gas pressure ranged from 0.5 to 4 mbar.

In our previous work [33], we discussed the confinement of plasma over the MC, which is represented by an abnormally glow discharge region. In region I, a potential  $V_p$  was applied to a single probe, resulting in a potential difference between the probe and plasma. Owing to the quasi-neutrality of the plasma, the fluxes of the positive ions and electrons toward the probe surface must be equal in the steady state. However, because electrons have a higher mobility than positive ions, the probe immersed in the plasma acquires a negative electrical charge. This leads to the establishment of an electric field that accelerates the positive ions and repels electrons. Consequently, the ion saturation current increased with increasing gas pressure [34].

After the transition to region II and the attainment of floating potential values, the single probe gradually became less negative and eventually positive. Just above the floating potential, the current increases exponentially (because the electron energy distribution is Maxwellian). This allows electrons to reach the probe, causing its potential to become even more positive in this region. In this region, the number of electrons collected by the probe exceeds the number of ions collected, owing to the higher mobility of electrons [35]. As

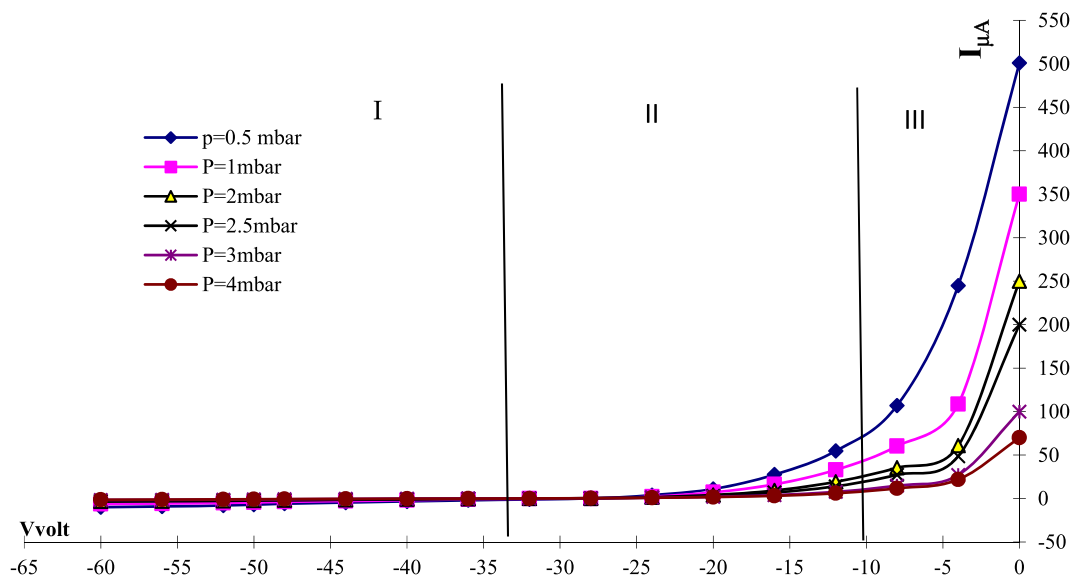


Fig. 5. The current-voltage characteristic curves of the single probe at a discharge current of 10 mA and an argon gas pressure ranging from 0.5 to 4 mbar, at axial region; 4 mm near the mesh cathode.

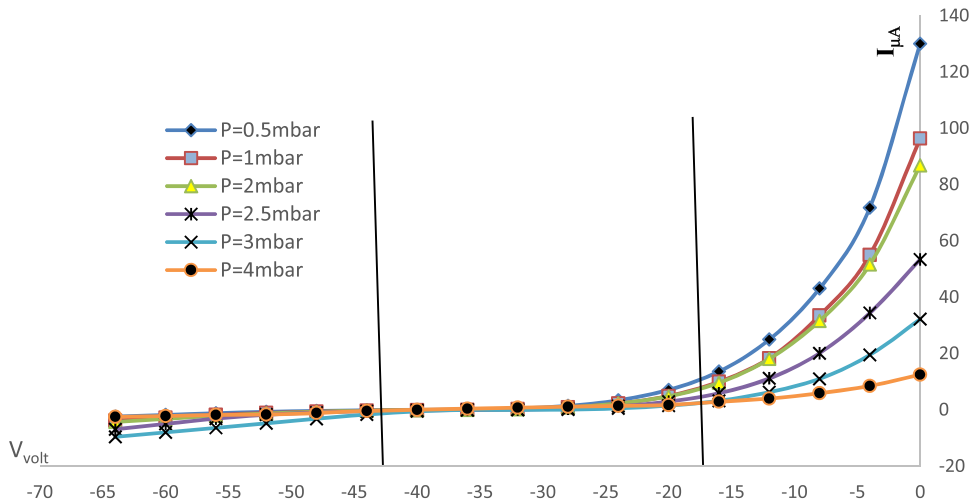


Fig. 6. The current-voltage characteristic curves of the single probe at a discharge current of 10 mA and an argon gas pressure ranging from 0.5 to 4 mbar, axially away from the MC further by 12 mm.

as a result, the probe current rapidly increased with increasing applied voltage. Only electrons with sufficient energy to overcome the sheath repulsion can reach the probe. It is worth noting that the electron saturation current ( $I_{\mu A}$ ) can be obtained when the sheath potential is zero, and its values are higher near the MC compared with the faraway axial distance [36].

### 3.3. The axial and radial distribution for the electron temperature

The current collected by the probe ( $I_{\mu A}$ ) versus the potential ( $V_p$ ) of the probe in transition region II from Figures (5) and (6) of the ( $I_a$ - $V_a$ ) characteristic of the single probe can be represented by the logarithm plot according to the single-probe theory [37]. This logarithmic plot formed a straight line with a slope of  $-(e/KT_e)$ . The electron temperature was determined by estimating the reciprocal of the slope as follows:

$$KT_e = \left[ \frac{d V}{d \ln(I)} \right] \tag{4}$$

The estimated temperature decreased as the pressure increased. This can be explained by the inverse relationship between the temperature and pressure, given by the following equation [38]:

$$|Te| = 6.5 |P^{-0.066}| \tag{5}$$

As the pressure increased, the breakdown voltage also increased, resulting in a higher electron density and a greater frequency of electron-electron collisions. These factors contribute to the decrease in electron temperature [39].

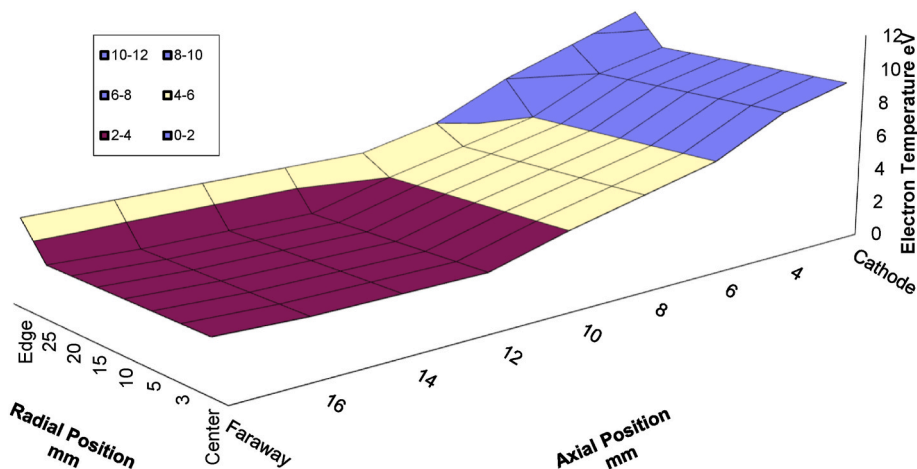


Fig. 7. 3-D distribution profile of the axial and radial electron temperature using the single Langmuir probe.

Furthermore, the electron density  $N_e$  increased as  $T_e$  decreased, where  $N_e$  can be calculated using the following equation:

$$N_e = \frac{I_{re}}{Aev_e} \tag{6}$$

Where  $I_{re}$ ,  $A$ ,  $e$ ,  $v_e$  are: the electron saturation current, the area of the probe, the electron charge, and the electron velocity respectively. All can be calculated using the following equation:

$$v_e = \sqrt{\frac{8KT_e}{\pi m_e}} \tag{7}$$

Fig. 7 shows the 3-D distribution profile of the axial and radial electron temperatures using the single Langmuir probe. The axial distribution reveals a sharp decrease in electron temperatures near the MC, with  $T_e$  values ranging from 8 to 9 eV, up to the abnormal glow discharge (at 12 mm) region, where  $T_e$  varies from 5 to 3 eV. Furthermore, in the faraway region,  $T_e$  varies from 0.5 to 2 eV.

Regarding the radial distribution, the temperatures remained relatively constant at approximately 2 eV within the same discharge region, except at the edge where it increased to 3.75 eV. This variation may be attributed to the non-uniform effect of plasma caused by the concentration of the electric field near the edge of the cathode, known as the “edge effect” [40].

Overall, the temperature values decreased from the MC to the axially away region, passing through the abnormal glow discharge region. Electrons emitted from the cathode surface gain energy and entered the abnormal glow discharge region, where they lose some energy through collisional excitation processes. The length of the abnormal glow discharge region is then determined by the dissipation of electron energy due to inelastic collisions with neutral atoms [41].

### 3.4. The axial and radial distribution for the electron density

Considering the inverse relationship between  $T_e$  and  $N_e$  values ( $T_e \times N_e = \text{constant}$ ) [42], it can be observed that the maximum value of one corresponds to the minimum value of the other. Fig. 8 shows the 3-D distribution profile of the axial and radial electron density exhibits a significant increase along the axial direction, starting from the MC region at 4 mm. The  $N_e$  values range from  $(3-4) \times 10^9 \text{ cm}^{-3}$  in this region and further increase to  $(10-12) \times 10^9 \text{ cm}^{-3}$  in the abnormal glow discharge region at 12 mm. As the axial distance increased, the  $N_e$  values sharply decreased to  $(0.5-1) \times 10^9 \text{ cm}^{-3}$  in the faraway axial distance range of (26–30) mm.

Additionally, Fig. 8 also illustrates the radial distribution of the electron density. The highest value of electron density, reaching  $15 \times 10^9 \text{ cm}^{-3}$ , was observed at the edge of the mesh cathode, resulting in bright and intense plasma. As the probe moved toward the abnormal region, the electron density gradually decreased to a moderate value of  $6 \times 10^9 \text{ cm}^{-3}$ . Finally, it sharply decreases toward the center, reaching a value of  $2 \times 10^9 \text{ cm}^{-3}$ . These decreases in electron density can be attributed to the ionization process that occurs after the breakdown of argon [43]. When electrons gain sufficient energy to ionize gas atoms, ionization occurs, causing a loss of energy in the electrons and an increase in their number. Moreover, an increase in pressure leads to an increase in the rate of ionization and, consequently, an increase in the number of electron-atom collisions.

### 3.5. Floating potential distribution

Optimal plasma surface treatment of polymers can be achieved by utilizing the high plasma density and low energy of electrons or

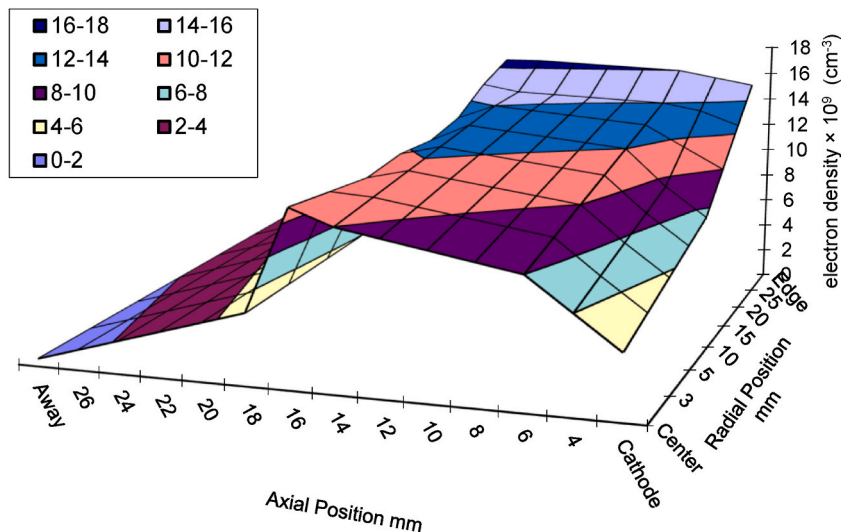


Fig. 8. 3-D distribution profile of the axial and radial electron density using the single Langmuir probe.

ions [44]. This can be accomplished by increasing gas pressure. The potential difference between the (n-WSF) (as a floating body) and plasma is referred to as the floating potential ( $V_f$ ), which is dependent on the electron temperature ( $T_e$ ). Floating potential  $V_f$  can be determined using the following equation [45]:

$$V_f = \frac{1}{2} \left[ \ln \left( 2\pi \frac{m_e}{m_i} \right) - 1 \right] \frac{KT_e}{e} \cong 3.34 \frac{KT_e}{e} \quad (8)$$

where  $k$  represents Boltzmann's constant,  $m_e$  represents the mass of an electron, and  $m_i$  represents the ion mass. The values of temperature  $T_e$  can be obtained from the measurements of the probe using the data from Figures (5 and 6). Fig. 9 illustrates the values of the axial floating potential distribution  $V_f$  at different applied pressures (1–4) mbar using equation (8). It shows a sharp axial decrement of the  $V_f$  at the MC, with a value of 13.5 eV, up to the abnormal glow discharge region (at 12 mm) with values ranging from 10 to 8 eV, and further faraway with values ranging from 6 to 4 eV. Moreover, as the temperature and floating potential decrease, plasma potential  $V_{\text{plasma}}$  also decreases, which can be calculated as follows [46]:

$$V_{\text{plasma}} = V_f + \frac{KT_e}{2} \left[ \ln \left( \frac{2m_i}{\pi m_e} \right) \right] \quad (9)$$

The floating potential is a critical factor for the floating sample (n-WSF), where fluctuations in the floating potential simply reflect changes in the plasma potential, local plasma density, and electron temperature [47,48]. Furthermore, there are various forces on the (n-WSF) sample, including electrostatic, gravitational, neutral, ion drag, and thermophoretic forces that influence inside low-pressure plasma (under vacuum) and satisfy a good medium for the inactivation process (see Table 1).

### 3.6. Optical emission spectroscopy (OES)

The emission spectra intensity of the DC glow discharge can be plotted against the wavelength, ranging from 200 to 900 nm, using the characteristics provided previously and are listed in Table 2. This allowed for the retrieval of OES data [49] of the DC glow discharge.

In the case of the argon-DC glow discharge, as depicted in Fig. 10, OES data were collected and are presented in Table 3, which includes information on the species elements, wavelength, intensity of emission spectra, and transitions for hydroxyl (OH), nitrogen bands ( $N_2$ ), and argon (Ar) with oxygen (O) radical lines. The presence of these bands and lines was attributed to the interactions of the Ar plume inside the chamber. The excited Ar species and high-energy electrons in the plasma interact with the surrounding ambient air [50].

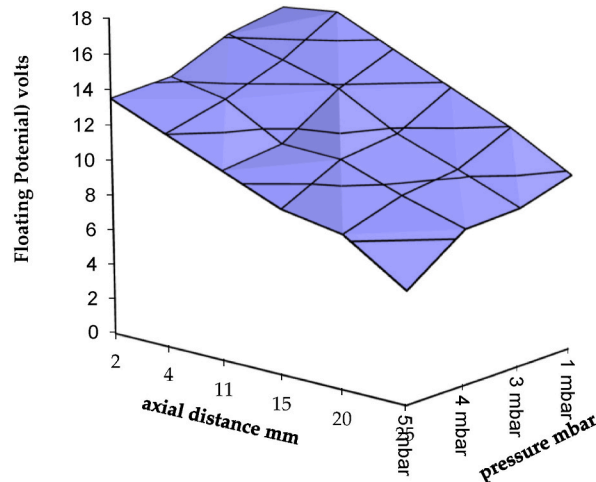
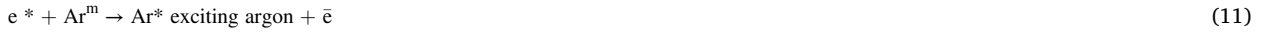


Fig. 9. 3-D distribution profile of the axial floating potential  $V_f$  at different applied pressures (1–4) mbar.



**Table 1**

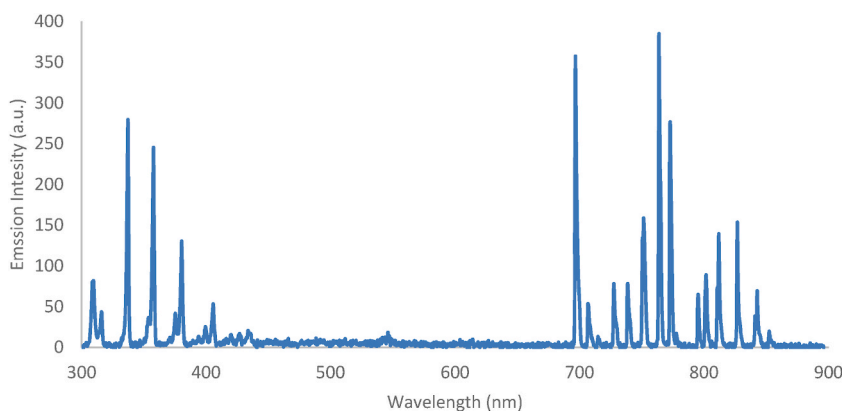
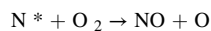
An experimental roadmap for the antimicrobial control by DC glow discharge measurements.

Experimental study of (n-WSF) using DC glow discharge	Electrical characteristics	a) Discharge current, from 4 up to 30 mA b) Discharge DC voltage, from 200 up to 1200 V c) Pressure, from 1 up to 5 mbar d) Current density, from 2 up to 15 mA/m <sup>2</sup>	Antimicrobial Control by DC glow discharge
	Plasma parameters	a) Potential distribution b) Electric field distribution c) Electron temperature d) Electron density e) Floating potential	
	Plasma distributions	a) Axial distribution b) Radial distribution	
	Optical emission spectroscopy	a) Detecting wavelengths lines and bands b) Detecting intensity emission spectra	
	Anti-microbial measurements	a) Survival curves of <i>E. coli</i> b) Exposure time	

**Table 2**

Measured characteristics for argon discharge.

Characteristic	Value	Unit
Low pressure plasma	DC glow Discharge	
Discharge current	4–30	mA
DC voltage	200–1200	volts
Pressure	1–5	mbar
Current density	2–15	mA/m <sup>2</sup>
Axial Position	Abnormal at 12 mm	
Electron temperature	5 to 3	eV
Electron density	10 to 12	x10 <sup>9</sup> cm <sup>-3</sup>
Floating potential	10 to 8	eV

**Fig. 10.** Intensity of emission spectra versus wavelength for argon DC glow discharge (low pressure plasma).

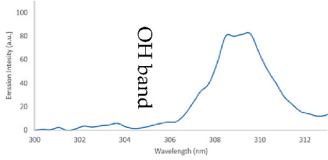
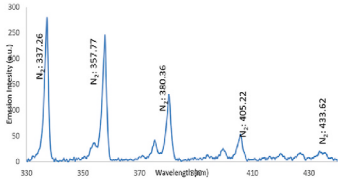
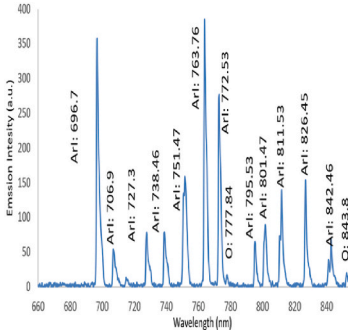
The emission of OH<sup>\*</sup> and O<sup>\*</sup> radicals can also occur as a consequence of impurities present in argon gas (commercial gas) or the infiltration of air into the discharge zone through the evacuation process [51]. Among the reactive species, O and OH are considered the most potent agents contributing to microbial inactivation of bacteria [52].

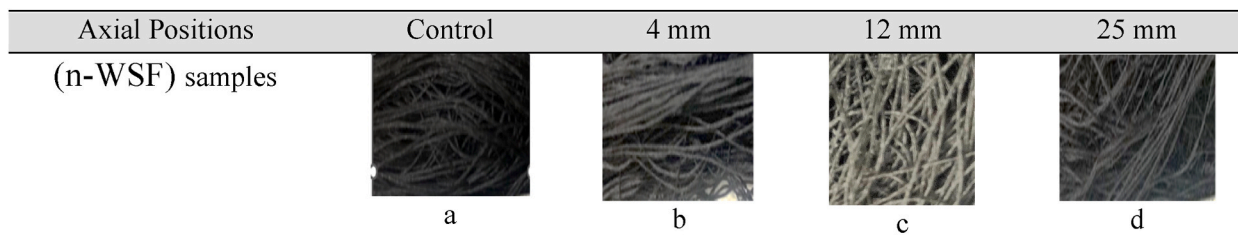
### 3.7. Survival curves

Fig. 11(a) displays a photograph of the control sample, while Fig. 11 (b, c, and d) show photographs of (n-WSF) samples treated

**Table 3**

Optical Emission Spectra data with corresponding species elements, wavelength, Intensity of emission spectra, and transitions for hydroxyl, with nitrogen bands, and Argon with oxygen lines.

Species	Wavelength (nm)	Intensity of emission spectra	Transition
OH band	309.6		$A^2\Sigma^+-X^2\Pi$
N <sub>2</sub> bands	3.15.37, 337.26, 357.77, and 380.36		$C^3\Pi_u-B^3\Pi_g$
Ar lines (O) lines	696.7, 706.9, 727.3, 738.46, 751.47, 763.76, 772.53, 795.53, 801.47, 811.53, and 826.45 777.84 and 843.8		$3s^23p^5(^2P^{\circ}_{3/2})4p$ $3s^23p^5(^2P^{\circ}_{3/2})4s$



**Fig. 11.** (a) Represents the control sample photo, and (b, c, and d) represent the treated (n-WSF) samples, with different applied axial distances from the MC of 4, 12, and 25 mm, respectively.

with various DC glow discharge controls at different distances from the MC: 4, 12, and 25 mm, respectively. The objective of this study was to analyze the survival curves of microorganisms attached to non-woven fabrics under direct-current glow discharge.

**Fig. 12(a)** shows the control Petri dish prior to treatment, containing a concentration of bacterial colonies of *E. coli* (CFU/mL). **Fig. 12 (b, c, and d)** illustrate the *E. coli* culture media after exposure to controls positioned at axial distances of 4, 12, and 25 mm from the MC, respectively. The deactivation regions within the Petri dish are indicated by an etched area, which initiates growth in the abnormal discharge region located 12 mm from the MC compared to the 4 mm position and 25 mm from the MC.

The survival curves presented in **Fig. 13** show the logarithm of the bacteria reduction R (CFU/ml) as a function of the exposure time, indicating that the bacterial reduction process and inactivation rate of (n-WSF) samples increased with increasing exposure time. The study also observed the survival data inside the Petri dish after the sputtering process and the amount of bacterial reduction [53]. The inactivation rate was found to increase because of the DC glow discharge plume. In this study, we identified three phases of bacterial spore inactivation.

Phases I, II, and III [54,55]. The survival curves for the axial position (12 mm) contained three phases, with death time values less than those for the axial positions of 4 mm and 25 mm owing to the low exposure time. The low treatment period, low pressure, low temperature, low floating potential, high density, and low dusty plasma were found to have the ability to produce a higher concentration of plasma over *E. coli* microbes and fast inactivation of bacteria at the axial position of 12 mm. Additionally, the exposure time was approximately halved when compared to the axial distances of 4 and 25 mm. Particulate contaminated DC glow discharges in the axial position of 4 mm, due to dust nanoparticle formation, delay the inactivation process [56,57], and the influence of the ambipolar-to-free diffusion transition on dust particle charge in a complex plasma [58] near the MC due to charging of dust grains in plasma with energetic electrons. Finally, a dramatic inhibitory effect of plasma discharge on the residual survival microbe ratio [59] in the abnormal region for the axial position of 12 mm was also observed. Finally, the optimal parameters of the axial position to 12 mm, the control region to the abnormal glow discharge region, and the low treatment period to 5.5 min for a complete inactivation process, which recommends maximum bacteria reduction when treating the n-WSF with the proposed discharge plasma sputtering device.

#### 4. Conclusion

The antimicrobial performance of the non-woven fabric under the electrical characteristics of direct current glow discharge was as follows: discharge current: 4–30 mA, discharge DC voltage: 200–1200 V, applied pressure: 1–5 mbar, and current density: 2–15 mA/m<sup>2</sup>. Axial and radial distributions of low-pressure plasma parameters, such as potential distribution, electric field distribution, electron temperature, electron density, and floating potential. Furthermore, plasma modes, such as optical emission spectroscopy, wavelength detection, and detection of intensity emission spectra, were discussed.

As the pressure increases, the breakdown voltage also increases, resulting in a higher electron density with a greater frequency of electron-electron collisions and contributing to a decrease in electron temperatures. These factors are satisfied in the abnormal glow discharge region suitable for the antimicrobial process of the (n-WSF).

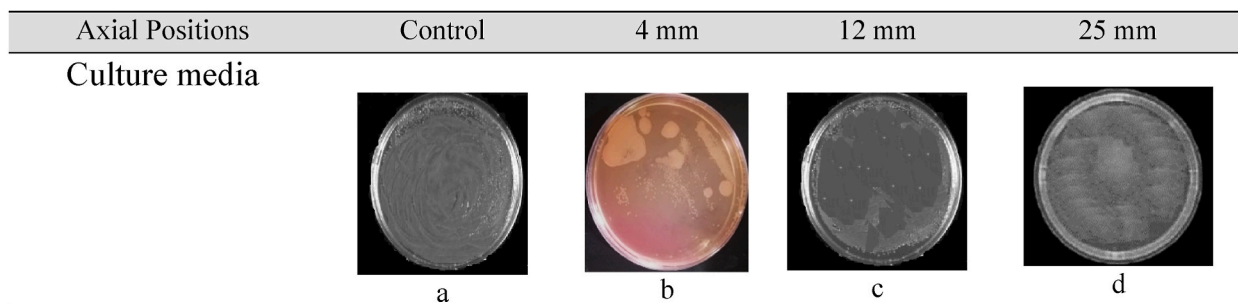


**Fig. 12.** (a) Represents the control Petri dish before treatment containing the bacterial colony concentration of *E. coli* (CFU/mL), and (b, c, and d) represent *E. coli* culture media after time exposure, and different applied axial distances from the MC of 4, 12, and 25 mm, respectively.

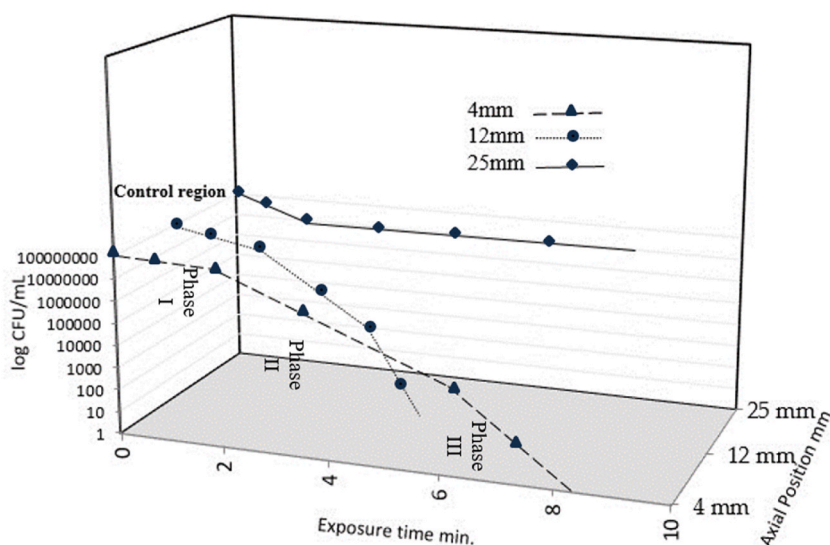


**Fig. 13.** 3-D distribution profile of the survival curves at different axial positions shows the logarithm of the bacteria reduction R (CFU/ml), as a function of the exposure time (min.).

The ideal plasma surface treatment for non-woven silk fabric (n-WSF) can be achieved by utilizing a high plasma density and low electron energy to effectively inactivate any viable cells attached to the fabric within optimal parameters for the axial position at 12 mm, the control region to the abnormal glow discharge region, and the low treatment period of 5.5 min for a complete inactivation process, which suggests maximum bacteria reduction when treating the n-WSF with the proposed discharge plasma sputtering device.

An analysis of the experimental data on the initial and final densities of viable cells using survival curves in the abnormal glow discharge region revealed a significant inhibitory effect on the residual survival microbe ratio due to the impact of plasma discharge.

From the perspective of future work, a comparison of the effects between the atmospheric pressure of the plasma jet and the direct current of glow discharge at low pressure (in vacuum) on the antimicrobial process of the (n-WSF).

**Institutional Review Board Statement:** Not applicable.

**Informed Consent Statement:** Not applicable.

## Funding

Deanship for Research & Innovation, Ministry of Education in Saudi Arabia for funding this research work through project number: IFP22UQU4250206DSR119.

## Additional information

No additional information is available for this paper.

## CRedit authorship contribution statement

**Ahmed Rida Galaly:** Writing – review & editing, Writing – original draft, Investigation, Funding acquisition, Formal analysis, Data curation, Conceptualization. **Nagia Dawood:** Supervision, Software, Resources, Project administration, Methodology.

## Declaration of competing interest

The authors declare the following financial interests/personal relationships which may be considered as potential competing interests: Ahmed Rida Galaly reports financial support was provided by Deanship for Research & Innovation, Ministry of Education in Saudi Arabia. If there are other authors, they declare that they have no known competing financial interests or personal relationships that could have appeared to influence the work reported in this paper.

## Acknowledgments

The authors extend their appreciation to the Deanship for Research & Innovation, Ministry of Education in Saudi Arabia, for funding this research work through project number IFP22UQU4250206DSR119.

## References

- [1] D. Morgan, K. Board, *An Introduction to Semiconductor Microtechnology*, John Wiley & Sons, Inc., New York, 1990.
- [2] N. Hershkowitz, R.A. Breun, *Diagnostics for plasma processing (etching plasmas, Rev. Sci. Instrum.* 68 (1997) 880.
- [3] D.A. Frank-Kamenetskii, *Plasma, the Fourth State of Material*, Plenum Press, 1972, pp. 11–18.
- [4] Ph Parker, *The Fundamentals of Gas Discharge Tubes Electronics*, Edward Arnold (Pub.) Ltd, 1963 (Chapter 15).
- [5] F.F. Chen, *Introduction to Plasma Physics and Controlled Fusion*, second ed., Plenum Press, 1984, p. 290.
- [6] W. Lochte-Holtgreven, *Plasma Diagnostics*, North Holland, Amsterdam, 1968, pp. 668–731.
- [7] R.H. Huddleston, S.L. Leonard, *Plasma Diagnostics Techniques*, Academic Press, New York, 1965, pp. 113–200 (Chapter 4).
- [8] B. Chapman, *Glow Discharges Processes J*, Wiley and Sons, New York, 1980.
- [9] Ahmed Rida Galaly, *Sustainable Development Solutions for the Medical Waste Problem Using Thermal Plasmas Sustainability* 14 11045, 2022, <https://doi.org/10.3390/su141711045>.
- [10] D. Ayhan, A. Gönenc, An overview of biomass pyrolysis, *Energy Sources* 24 (2002) 471–482.
- [11] Vishwajeet, H. Pawlak-Kruczek, M. Baranowski, M. Czerep, A. Chorażyczewski, K. Krochmalny, M. Ostrycharczyk, P. Ziółkowski, P. Madejski, T. Mączka, et al., Entrained flow plasma gasification of sewage sludge—proof-of-concept and fate of inorganics, *Energies* 15 (2022) 1948.
- [12] M. Liu, Q. He, J. Bai, J. Yu, L. Kong, Z. Bai, H. Li, C. He, X. Cao, Z. Ge, et al., Char reactivity and kinetics based on the dynamic char structure during gasification by CO<sub>2</sub>, *Fuel Process. Technol.* 211 (2021) 106583.
- [13] Z. Chen, G. Garcia Jr., V. Arumugaswami, R.E. Wirz, Cold atmospheric plasma for SARS-CoV-2 inactivation, *Phys. Fluids* 32 (2020) 111702.
- [14] L. Zhang, Y. Guo, X. Chang, Z. Yao, X. Wei, Z. Feng, D. Zhang, Q. Zhou, X. Wang, H. Luo, In-Duct grating-Like dielectric barrier discharge system for air disinfection, *J. Hazard Mater.* 435 (2022) 129075.
- [15] A.H. Asghar, Rida Galaly Ahmed, *The Influence of Different Plasma Cell Discharges on the Performance Quality of Surgical Gown Samples Materials*, vol. 14, 2021, p. 4329.
- [16] Rida Galaly Ahmed, N. Dawood, *Non-Thermal Plasma Treatment Coupled With a Photocatalyst for Antimicrobial Performance of Ihram Cotton Fabric Nanomaterials* 12 1004, 2022, <https://doi.org/10.3390/nano12061004>.
- [17] H. Morris, R. Murray, Modeling the effect of weave structure and fabric thread density on the barrier effectiveness of woven surgical gowns Medical textiles, *Textil. Prog.* 52 (2020) 1–127.
- [18] M. Laroussi, Low Temperature Plasma-Based Sterilization: Overview and State-of-the-Art *Plasma Proc. Polym* 2 (5) (2005) 391.
- [19] I.O. Soloshenko, V.A. Khomich, V.V. Tsiolko, et al., in: *Theoretical and Experimental Study of the Factors of the Sterilization of Medical Articles in Low Pressure Glow Discharge Plasma Proceedings of the 14<sup>th</sup> International Symposium on Plasma Chemistry*, Prague August, vols. 2–6, 1999, pp. 2551–2556.
- [20] D. Bohm, *The Characteristics of Electrical Discharge in Magnetic Fields* Guthrie A and Wakerling R.K, McGraw-Hill, New York, 1949.
- [21] A.R. Galaly, The effect of different cathode configurations of the plasma cell on the ion velocity distribution function, *IEEE Trans. Plasma Sci.* 49 (2) (2021) 535–545, <https://doi.org/10.1109/TPS.2020.30374>.
- [22] R.L. Merlino, Understanding Langmuir probe current – voltage characteristics, *Am. J. Phys.* 75 (12) (2007) 1078–1085.
- [23] G. Guethlein, T. Houck, J. McCarrick, S. Sampayan, Faraday cup measurements of ions backstreaming into a electron beam impinging on a plasma plume, in: *Proceedings of Linear Accelerator Conference, Monterey, 21- 25 August, 2000*, pp. 467–469.
- [24] A. Rida Galaly, F.F. El Akshar, M. Atta Khedr, Study of the Etching Processes of Si [1 0 0] Wafer Using Ultra Low-Frequency Plasma *Materials Science Forum* 756 (2013) 143.
- [25] A. Rida Galaly, Gap mesh wire control on nano-particles growth, *J. Mod. Phys.* 6 (2015) 1162.
- [26] E.S. Allehyani, Surface functionalization of polyester fabric for antibacterial and antioxidant properties, *Polymers* 14 (2022) 5512, <https://doi.org/10.3390/polym14245512>.
- [27] S.I. Siddiqui, E.S. Allehyani, S.A. Al-Harbi, Z. Hasan, M.A. bomuti, H.K. Rajor, Investigation of Congo red toxicity towards different living organisms, *Rev. Processes* 11 (807) (2023). <https://doi.org/10.3390/pr11030807>.
- [28] R. Morent, N. De, Inactivation of Bacteria by Non-Thermal Plasmas, *Biomedical Engineering - Frontiers and Challenges InTech*, 2011, <https://doi.org/10.5772/18610>.
- [29] OB Ahmed, AH Asghar, M Bamaga, FS Bahwerth, M.E. Ibrahim, Characterization of aminoglycoside resistance genes in multidrugresistant Klebsiella pneumoniae collected from tertiary hospitals during the COVID-19 pandemic, *PLoS One* 18 (7) (2023) e0289359, <https://doi.org/10.1371/journal.pone.0289359>.
- [30] A. Alisaac, M. Alsahag, M. Alshareef, R.M. Snari, M. Alhasani, H.M. Abumelha, N.M. El-Metwaly, Development of smart cotton fabrics immobilized with anthocyanin and potassium alum for colorimetric detection of bacteria, *Inorg. Chem. Commun.* 145 (2022) 110023. <https://doi.org/10.1016/j.inoche.2022.110023>.
- [31] X. Lu, T. Ye, Y.G. Cao, Z.Y. Sun, Q. Xiong, Z.Y. Tang, Z.L. Xiong, J. Hu, Z.H. Jiang, Y. Pan, The roles of the various plasma agents in the inactivation of bacteria *J. Appl. Phys.* 104 (5) (2008) 053309.
- [32] M. Laroussi, D.A. Mendis, M. Rosenberg, Plasma interaction with microbes, *New J. Phys.* 5 (2003) 41, <https://doi.org/10.1088/1367-2630/5/1/341>.
- [33] A. Rida Galaly, G. Van Oost, Comparison between theoretical and experimental radial electron temperature profiles in a low density weakly ionized plasma," *J. Mod. Phys.* 10 (7) (2019) 699.
- [34] R.M. Snari, M. Alsahag, A. Alisaac, A. Bayazeed, A. Alsoliemy, M.E. Khalifa, N.M. El-Metwaly, Smart textiles immobilized with hydrazone probe for colorimetric recognition of bacteria, *J. Mol. Liq.* 366 (2022) 120149. <https://doi.org/10.1016/j.molliq.2022.120149>.
- [35] E. Eser, R.E. Ogilvie, Measurement of plasma discharge characteristics for sputtering applications, *J. Vac. Sci. Technol.* 15 (1979) 199.
- [36] A. Bogaerts, et al., Gas discharge plasmas and their applications *Spectrochimica Acta* 57 (2002) 609.
- [37] V.I. Demidov, S.V. Ratynskaia, K. Rypdal, Electric probes for plasmas: The link between theory and instrument, *Rev. Sci. Instrum.* 73 (2002) 10, <https://doi.org/10.1063/1.1505099>.
- [38] A. Klimov, A. Zenin, E. Oks, Plasma density distribution in a plasma source of a ribbon electron beam with an extended hollow cathode, in: *AIP Conference Proceedings* 1899, 2017 040007.
- [39] A. Von Engel, *Ionized Gases*, Oxford, 1965.
- [40] Ahmed Rida Galaly, The edge effect on the EEDF measurements of magnetized DC plasma, *Br. J. Appl. Sci. Technol.* 11 (3) (2015) 1.
- [41] A. Nikolay, Z. Yury, P. Anatoly, *Influence of Nitrogen Admixture on Plasma Characteristics in a Dc Argon Glow Discharge and in Afterglow* *Atoms*, 7 13 1, 2019.
- [42] T. Matsoukas, M. Russell, Particle charging in low-pressure plasmas, *J. Appl. Phys.* 77 (1995) 4285.
- [43] B. Doggett, J.G. Lunney, *Langmuir probe characterization of laser ablation plasmas*, *J. Appl. Phys.* 105 (2009) 033306, <https://doi.org/10.1063/1.3056131>.
- [44] H. Turkoglu Sasmazel, M. Alazzawi, N. Kadim Abid Alsaheb, Atmospheric Pressure Plasma Surface Treatment of Polymers and Influence on Cell Cultivation, *Molecules* 17 26 (6) (2021) 1665, <https://doi.org/10.3390/molecules26061665>.
- [45] F.F. Chen, *Electric Probes, Plasma Diagnostic Techniques* R.H. Huddleston and S.L. Leonard, 1965. New York City, NY.
- [46] I.H. Hutchinson, *Principles of Plasma Diagnostics* Cambridge, 2005, pp. 53–64. U.P. New York City NY.
- [47] L.A. Berni, M. Ueda, G.F. Gomes, A.F. Beloto, H. Reuther, Experimental results of a dc glow discharge source with controlled plasma floating potential for plasma immersion ion implantation, *J. Phys. D Appl. Phys.* 1592 13 (33) (2000), <https://doi.org/10.1088/0022-3727/33/13/306>.
- [48] Sudeshna Lahiri, et al., Study of the floating potential in a glow discharge plasma using Langmuir Probe, *International Journal of Research on Social and Natural Sciences* 2 (2) (2017) 2455–5916.
- [49] See <https://www.nist.gov/pml/atomic-spectra-database> for “NIST Atomic Spectra Database” (last accessed August 21, 2020).
- [50] L.F. Dong, Y.Y. Qi, Z.C. Zhao, Y.H. Li, X.C. Li, Study on energy transfer in argon/air in dielectric barrier discharge by optical emission spectra, *Guang Pu Xue Yu Guang Pu Fen Xi* 28 (11) (2008) 2491. Chinese. PMID: 19271473.

- [51] W.J. Wang, et al., Visible-Light-Driven photocatalytic inactivation of E. coli K-12 by bismuth vanadate nanotubes: bactericidal performance and mechanism, *Environ. Sci. Technol.* 46 (2012) 4599.
- [52] J. Shen, et al., Sterilization of *Bacillus subtilis* spores using an atmospheric plasma jet with argon and oxygen mixture gas, *APEX* 5 (2012) 3.
- [53] Rida Galaly Ahmed, H.H. Zahran, Inactivation of bacteria using combined effects of magnetic field, low pressure, and ultra low-frequency plasma discharges (ULFP), *J. Phys. Conf. Ser.* 431 (2013) 012014.
- [54] M.J. Kushner, J.T. Michael, Caughey, A model for particulate contaminated glow discharges, *J. Appl. Phys.* 69 (10) (1991) 6952.
- [55] B. Walch, M. Horányi, S. Robertson, *Charging of dust Grains in Plasma with energetic electrons* 1995, *Phys. Rev. Lett.* 75 (1995) 838.
- [56] L. Couédel, A.A. Samarian, M. Mikikian, L. Boufendi, *Influence of the Ambipolar-to-free Diffusion Transition on Dust Particle Charge in a Complex Plasma Afterglow* *Physics of Plasmas*, vol. 15, 2008 063705.
- [57] A. Michau, et al., Nanoparticle formation and dusty plasma effects in DC sputtering discharge with graphite cathode, *Plasma Sources Sci. Technol.* 25 (2016) 15019.
- [58] Z. Buntat, et al., Generation of a homogeneous glow discharge: a comparative study between the use of fine wire mesh and perforated aluminum electrodes, *Appl. Phys. Res.* 3 (2011), 1 201115.
- [59] René Pompl, et al., The effect of low-temperature plasma on bacteria as observed by repeated AFM imaging, *New J. Phys.* 11 (2009), 115023 1.